Proc. Natl. Acad. Sci. USA
Vol. 93, pp. 6037–6042, June 1996
Neurobiology

Magnetic resonance imaging (MRI) detection of the murine brain response to light: Temporal differentiation and negative functional MRI changes

WEI HUANG†‡§, ILDIKÓ PÁLYKA†‡, HAIFANG LI¶, EDWARD M. EISENSTEIN¶‖, NORA D. VOLKOW**, AND CHARLES S. SPRINGER, JR.†‡¶

Departments of †Chemistry and ¶Radiology, State University of New York, Stony Brook, NY 11794; ‖Department of Radiology, Veterans Affairs Medical Center, Northport, NY 11768; Departments of ‡Chemistry and **Medicine, Brookhaven National Laboratory, Upton, NY 11973; and §Laboratory of Neurosciences, National Institute on Aging, National Institutes of Health, Bethesda, MD 20892

Communicated by Alfred P. Wolf, Brookhaven National Laboratory, Upton, NY, November 30, 1995 (received for review June 15, 1995)

ABSTRACT **Using a 9.4 T MRI instrument, we have obtained images of the mouse brain response to photic stimulation during a period between deep anesthesia and the early stages of arousal. The large image enhancements we observe (often >30%) are consistent with literature results extrapolated to 9.4 T. However, there are also two unusual aspects to our findings. (*i*) The visual area of the brain responds only to *changes* in stimulus intensity, suggesting that we directly detect operations of the M visual system pathway. Such a channel has been observed in mice by invasive electrophysiology, and described in detail for primates. (*ii*) Along with the typical positive response in the area of the occipital portion of the brain containing the visual cortex, another area displays *decreased* signal intensity upon stimulation.**

It has been found that the signal-to-noise ratio (S/N) of the neural responses to stimuli observed in functional magnetic resonance imaging (fMRI) increases supralinearly with the static magnetic field strength (measured as flux density, $\mathbf{B}_0$) (1), as apparently also does the spatial focus to the actual sites of brain metabolism (2). The largest value of $\mathbf{B}_0$ currently used for humans is 4.1 T (3). Higher field MRI instruments do exist but are constrained to the study of animals by their magnet bore sizes. Of course, animals must be immobilized (anesthetized and/or paralyzed) for such investigations. In a separate report (4), we have shown that although the large dose of pentobarbital anesthetic required initially inhibits a detectable murine brain response to visual stimulation, there is a time window following a bolus administration when growing brain responses can be detected, before motion artifacts attendant to arousal preclude fMRI.

We report here studies conducted during this time window. We have explored 9.4 T fMRI signals in the occipital region of the mouse brain in response to a flashing, point light source, which was also varied in the duration of illumination. Preliminary results have been presented in abstract form (5–8), including responses to olfactory and whisker-motor stimulations (5).

METHODS

In our experiments, male Swiss–Webster (albino) mice (30–35 g; Taconic Farms; $n \approx 45$) were anesthetized with sodium pentobarbital (60–65 mg/kg, bolus i.p. injection). To avoid impractical mechanical ventilation, no expressly paralytic drug was administered. Each animal was positioned rostral end down in a Bruker imaging probe, its head resting in an 18-mm-diameter cylindrical glass support inside the 25-mm-diameter saddle-shaped transceiver coil, in which the brain was centered. A Bruker MSL 400 instrument equipped with a 9.4 T magnet having a (vertical) free-bore of 89 mm diameter was controlled by an ASPECT 3000 computer. Inside the magnet, the animal was ventilated by a stream of air with a flow set to ≈7 liters/min at the MSL temperature control unit. The transceiver coil was tuned and matched at 400.2 MHz.

On a few individuals, sets of thin-sliced (thickness, nominally 0.7 mm), high-resolution (256 × 256 matrix size) coronal images were obtained that covered the entire brain region. A simple low flip-angle ($\alpha = 25°$) gradient echo pulse sequence was used. The field-of-view was $(30\ \text{mm})^2$. The echo time (TE) (2.5 ms) and repetition time (TR) (500 ms) values were set to yield images that were mostly spin density-weighted, with a relatively high S/N from the thin slices. Each image required ≈2.1 min to acquire. They were compared to anatomical photographs in a mouse brain atlas (9) to serve as references for the fMRI slice selections.

For the fMRI experiments, one end of a coated 1-mm-diameter optical fiber (Edmund Scientific, Barrington, NJ) had been inserted through the air tunnel in the bottom of the probe, into the coil area, and taped to the inner support wall. After the mouse was positioned, the end of the optical fiber was 5–8 mm away from the open eyes of the anesthetized animal. The other end of the optical fiber was located 1–5 mm away from the end of the output cable of a white light source (Reichert Scientific; 150 W bulb). The latter was controlled by an electronic switch that caused the light to flash, stroboscopic-like, at 7 Hz. When not flashing, the light power, measured at the end of the output cable, was set at either 0.60 ± 0.01 or 0.30 ± 0.01 W.

At the beginning of each fMRI experiment, high (256 × 256) or intermediate (128 × 128) resolution scout coronal brain images were acquired in 25 or 12 s, respectively, in order to locate the visual area by comparison with the spin-density images. A phase-refocused, steady-state free precession, fast gradient echo imaging sequence (10) was employed, with signal detection on only the second echo to provide maximal T_2^*-weighting. Because of the loss of signal intensity due to the latter, the slice thickness of these images was increased to 2 mm. Other parameters included $\alpha = 25°$, field-of-view = $(30\ \text{mm})^2$, TE = 3 ms (for the second echo), and TR = 85 ms. Once the appropriate slice was selected, the visual stimulations were performed during the acquisition of a "movie" of 32 images, with the same parameters as for the scout images except for a smaller data matrix (128 × 64), longer TE (11 ms), and shorter TR (13 ms). Each movie image was collected in ≈0.9 s, and there was usually no delay between images. Before any stimulations, a movie was always obtained to ensure that a steady baseline of image intensity could be observed. As we reported elsewhere (4, 7), movie data collections could be profitably started ≈1 h after the anesthetic injection (postanesthetic;

The publication costs of this article were defrayed in part by page charge payment. This article must therefore be hereby marked "*advertisement*" in accordance with 18 U.S.C. §1734 solely to indicate this fact.

Abbreviations: MRI, magnetic resonance imaging; fMRI; functional MRI; S/N, signal-to-noise ratio; PA, postanesthetic; ROI, region of interest; BOLD, blood oxygenation level dependent.

PA), and continued until the animal was aroused enough that motion artifacts blurred the signal change resulting from the visual stimulation (typically, ≈2.5 h PA).

A few movies were collected with 3-s interimage delays to confirm that there was no change in the pattern of brain response; for example, due to the stimulation-induced inflow of fresh, unsaturated blood spin magnetization (11). The lack of significant dependence of the results on α (between 15° and 35°) also suggested little such effect in our case.

Photic stimulations were performed by using the following protocols (with the laboratory lighting extinguished). (*i*) The length of the stimulation period was systematically varied from a value of ≈3.6 s (time for collecting 4 images) up to ≈18 s (time for collecting 20 images), with constant intensity (0.6 W) and frequency (7 Hz). (*ii*) The light intensity was very quickly increased or reduced in the middle of 14.4-s stimulations.

After each movie acquisition, the images were examined for intensity changes due to the brain response by using Bruker software and the ASPECT 3000 computer. The mean signal intensities of arbitrarily selected square regions of interest (ROIs) [between 18 and 72 (12 × 6) rectangular pixels in extent] from a movie's images were plotted as a function of time. A sufficient number of different ROIs were studied so that the entire brain region was effectively examined. (The 72-pixel ROI comprises ≈8 mm^2, or ≈0.2 of the brain area visible.) Movie image data were then transferred onto a VAX-station/3100 computer where image processing (mainly image algebra) was carried out with a specially written FORTRAN program using GIFA (Oxford Molecular, Paliseau, France) routines for image display (12). Simple difference (a movie image with maximum signal intensity change minus a movie image with baseline intensity) images were displayed with a seven-color scale that measures percent intensity change relative to that of the pixel with the greatest intensity in the baseline image. For presentation, the difference images were superimposed onto the gray-scale scout image of the same brain slice by using POSTSCRIPT programming.

The use of simple difference images is reasonable in this work. Due to the small number of baseline (computer-limited to typically 20) and "activated" (usually one, for each response) images we can obtain in a single movie, an extensive statistical analysis of our data is not warranted. However, the high field of our instrument (9.4 T) provides us with the large signal intensity changes (increases often >30%) expected. For example, only pixels with intensity changes in excess of ±7% are shown in fMRIs depicted in this paper (see Fig. 4). At this level (above the maximum observed in low-field studies), the reproducibility of the functional maps is quite high: "noise" is rarely seen. In the fMRIs, the absolute value of the standard deviation of the baseline intensities of individual pixels (in percent signal change) is 1.27% (see Fig. 4). Changes larger than ±5% (below the cutoff threshold) are <0.1% likely to arise from random fluctuations. The possibility of mistaken identification of motion artifacts was eliminated by a computer-generated superimposition and examination of the individual movie images (see below).

In the ROI intensity time-course plots, the absolute values of the standard deviations of the baseline intensities (in percent signal change) ranged from 3.65% (see Fig. 3*a*, open symbols) to 5.80% (see Fig. 3*a*, filled symbols). The peak intensities during responses are well within the 99.9% confidence interval in all cases except those of the open symbols in Fig. 3*b*, and even the latter are >95% likely not to arise from random fluctuations.

RESULTS

Fig. 1 displays 6 of 12 high-resolution (256 × 256) anatomical coronal images obtained from a mouse in order to locate the fMRI slice in the brain anatomy. Each is viewed from an anterior position and the twelve are numbered consecutively from anterior to posterior. The approximate locations of the six images are indicated by vertical lines drawn on an adaptation of a midsagittal view of the (C57BL/6J strain) murine brain in the skull (9). The locations were estimated by comparison of the images with photographs of stained coronal brain slices (9), from a knowledge of the average murine brain dimension (see the scale bar for the midsagittal view in Fig. 1), and from the thickness (0.7 mm) and contiguity (nominal center-to-center spacing, 0.8–0.9 mm) of our anatomical image slices. The thicknesses are indicated by the horizontal bars in the center of Fig. 1, although these also probably serve as reasonable estimates of location uncertainty as well. Although the vertical lines suggest perfectly coronal planes, the image slices could be slightly skewed, in the pitch and/or yaw senses. The same is true for our scout and functional images. The final position of the mouse inside the gradient coils cannot be perfectly controlled or well observed. Sagittal MR images of the mouse brain are not practical with our set up.

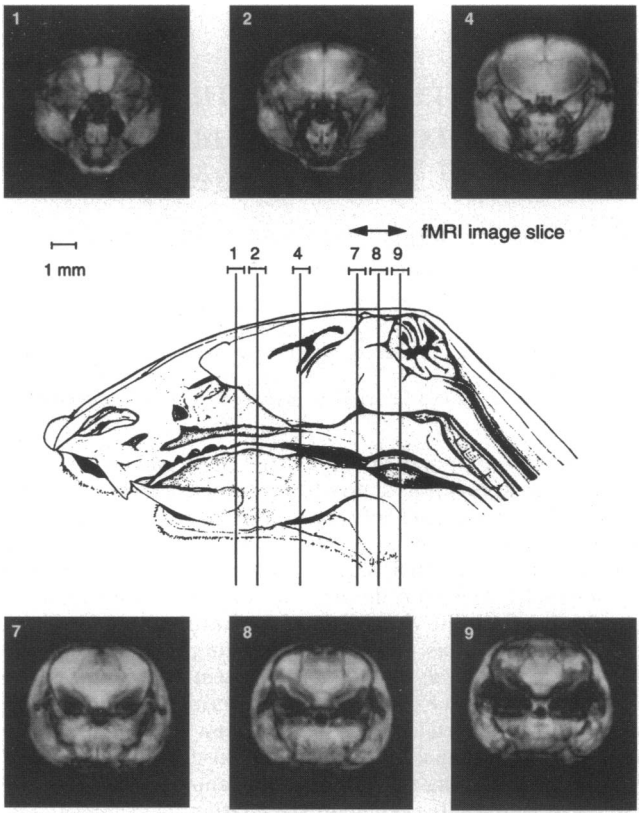

FIG. 1. Six of 12 coronal anatomical (256 × 256) images of a mouse head are shown. The view perspective is from an anterior position. The approximate locations of the image slices are indicated by the vertical lines in the middle of the figure, along with their thicknesses. The lines are superimposed on the midsagittal view of the mouse head adapted from ref. 9. The 12 contiguous slices encompassed the entire brain. The approximate location of the thicker slice used for fMRI in this work is also indicated. It roughly comprises anatomical slices 7, 8, and 9 and is situated mostly anterior to the cerebellum.

It is important to note that the coronal images seen in Fig. 1 include the entire head. Thus, for example, the small dark void near the center of image 4 represents the trachea, and the mass below it a section of the hypoglossus. On either side of the latter are seen sections of the masseter muscles (not present in the midsagittal view). The brain section occupies approximately the top one-third pie-shaped portion of the circular image.

The location of the fMRIs, as well as their thickness, is indicated in the midsagittal view portion of Fig. 1. An fMRI slice roughly corresponds to the combination of anatomical

slices 7, 8, and 9. Thus, it comprises a 2-mm-thick coronal section mostly anterior to the cerebellum. This encompasses most of the primary visual cortex (area 17, striate cortex) and the extrastriate visual regions immediately adjacent to it (area 18a, extending lateral and anterior to area 17; and area 18b, lying medial to area 17) (13). Three sinus-caused signal voids are quite prominent in the image of slice 9. The superior pair most likely represents ear cavities. The third is surely the esophagus.

Fig. 2 shows temporal plots of the changes of the mean signal intensity of the pixels in fMRI ROIs containing positively enhanced areas (see below). The dashed curves are meant only to guide the eye. As is evident, the observable magnetization generally reaches a steady-state level after the first 3 to 4 s of a movie. The 0.6-W stimulations are represented by the step function envelopes at the bottoms of the plots. (A wave form depicting the 7-Hz oscillation is seen in the top envelope of Fig. 2.) Brain responses similar to those in Fig. 2 were also observed when longer delays (3 s) were used between movie images. In other experiments (not shown), we have also found that the intensity of the response to a 4.5-s stimulation decreases if the intensity of the light is reduced to 0.3 W or the flashing frequency to 2 Hz.

Fig. 2 also displays the dependence of the response on the stimulation duration. The intercept of the baseline of each plot on the overall ordinate represents the time elapsed PA, at the beginning of data acquisition. Thus, over a relatively brief period of time (≈25 min), the stimulation length was varied from 3.6 to 13.5 s (time for collecting 4 and 15 images, respectively). When the duration exceeds a value between 5.4 and 7.2 s (time for collecting 8 images), second and third plots, the response becomes clearly bimodal; correlating with the times that the light source is switched on and off, respectively. Typically, the response rises in less than a second after the beginning of the stimulation. Certainly by the time the stimulation is 7.2 s long, the initial response has declined to the baseline in 4 s. A very similar response is observed when the stimulus is switched off. The responses to the two shortest stimulations (top of Fig. 2) show some evidence of structure.

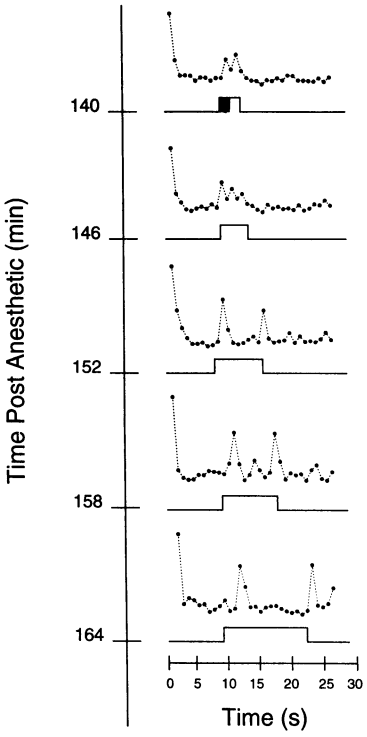

FIG. 2. The effect of stimulation time on the fMRI response is shown. The duration of (7 Hz) photic stimulations was increased from 3.6 s to 5.4, 7.2, 9.0, and 13.5 s (top to bottom) for a single mouse. These are indicated by the step function envelopes drawn at the bottoms of the plots. The intercept of a baseline on the overall ordinate gives the time elapsed since the administration of sodium pentobarbital anesthetic, at the beginning of that stimulation experiment. Dashed lines are intended only to guide the eye.

The increasing intensity of the responses with time elapsed PA also evident in Fig. 2 is quite reproducible. The local ordinates for each of the plots (not shown) have identical scales. In other reports (4, 7), we have quantified this phenomenon and discussed its importance.

Fig. 3 demonstrates that besides responding to the beginning and the ending of the stimulation, the mouse brain also responds to sudden isochromatic changes of light intensity during the course of the stimulus (7 Hz, 14.4-s duration). The response is the same whether there is a *decrease* in light intensity (from 0.6 to 0.3 W), applied ≈130 min PA (Fig. 3*a*), or an *increase* (from 0.3 to 0.6 W), applied to another mouse ≈170 min PA (Fig. 3*b*). There are plots in Fig. 3 for data from ROIs exhibiting *negative* fMRI responses (open circles), as well as from those encompassing the major positive changes (filled circles). The intensity changes are adjusted so that the mean ROI pixel intensity of the average baseline image is zero. In Fig. 3, there is no evidence of structure in the "on" responses. Perhaps these mice were closer to arousal.

Fig. 4 presents images from the experiment of Fig. 3*a*. Fig. 4*a* displays a high-resolution (256 × 256) scout image of the mouse obtained before stimulation. Difference images are

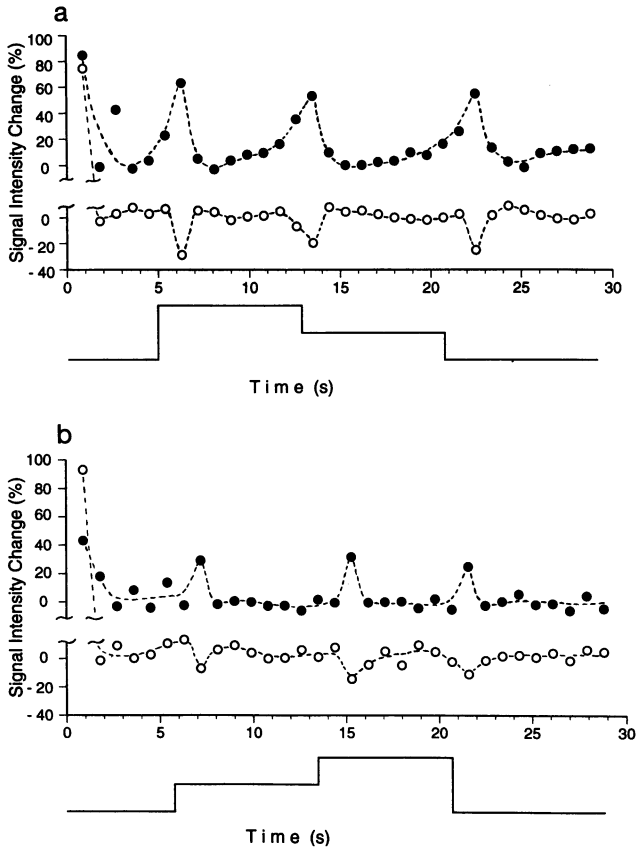

FIG. 3. Time courses of fMRI changes in response to more complicated photic stimulation protocols are shown. (*a*) Results of an experiment on one mouse for which the light intensity was decreased midway through a 14.4-s (7-Hz) stimulation. (*b*) Results for an experiment on a different mouse in which the light intensity was increased. The stimulations are indicated by the step function envelopes shown at the bottoms of the plots. ●, Average changes of pixels in ROIs that included the areas of image enhancement; ○, average changes in ROIs encompassing foci of decreased intensity. Dashed lines are intended only to guide the eye.

overlaid onto the image of Fig. 4*a* and shown in Fig. 4 *b–f*. The difference images are displayed in color, and the color scale percentage values represent 100 $[(S - S_0)_p/S_{0,max}]$, where S is the signal intensity in the image acquired during activation, S_0 is the signal intensity in the baseline image, p is the pixel index, and $S_{0,max}$ is the intensity of the baseline image pixel with maximum signal. The ROI with the major increase in intensity is mostly on the left side of the brain slice displayed (the right side of the image). This is generally what we observe for most mice. However, there are noticeable variations, possibly a feature of the particular centering and orientation of these slices that—although thin in conventional MRI terms—are thick relative to the tiny mouse brain. An ROI with decreased intensity is seen near the superior portion of the brain slice, and reasonably centrally located.

Fig. 4*b* shows the areas for this mouse that were activated ≈1 s after the light was switched on, Fig. 4*c* presents the difference image obtained ≈3.6 s since the light had been turned on, while Fig. 4*d* depicts the areas responding ≈1 s after the light intensity decrease. Fig. 4*e* shows the difference image obtained ≈3.6 s after the decrease in light intensity and Fig. 4*f* depicts the areas responding ≈2.7 s since switching off of the light. Fig. 4 *c* and *e* demonstrate that the brain has "accommodated" to the *continuing* stimulus, showing no response. The three response patterns (Fig. 4 *b*, *d*, and *f*), including both the negative and positive changes, are essentially the same. This is what we usually observe. (Note that the percentage scales in Figs. 3*a* and 4 were calculated differently, as described above.)

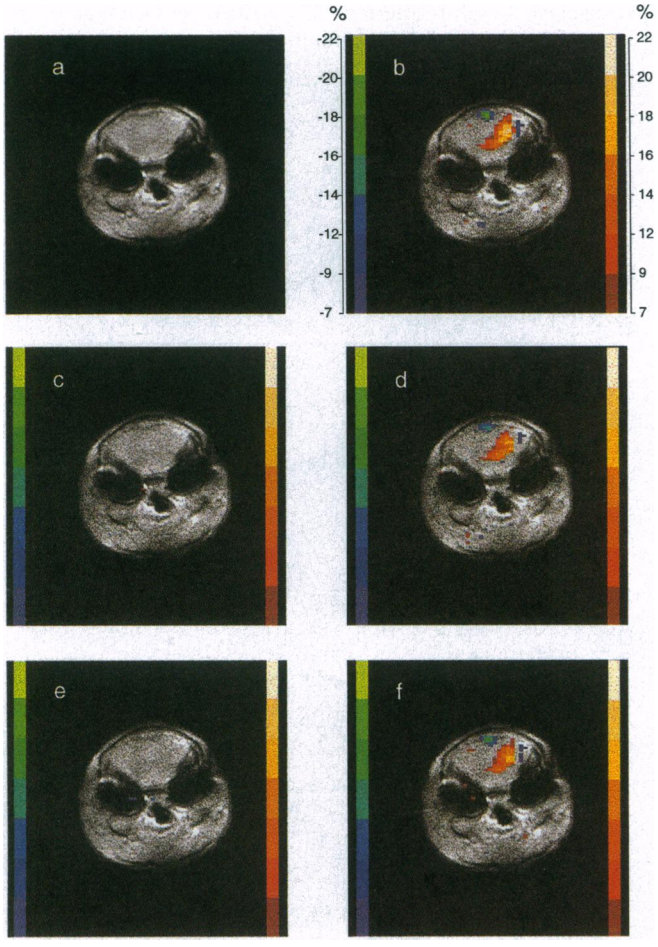

FIG. 4. Coronal images from the experiment of Fig. 3a are shown. A 256 × 256 image obtained before stimulation is seen in *a*. In the other panels, color-coded fMRI difference images are superimposed on the gray-scale scout image. The color scales are given on either side of these images. *b–f* show the images obtained 1, 3.6, 8.1, 10.7, and 17.1 s after the light was switched on, respectively. Thus, *b*, *d*, and *f* show the responses to the switching on, the decrease in intensity, and the switching off of the light, respectively. On the other hand, *c* and *e* show the "accommodation" of the mouse brain to the continued stimulation.

No response to stimulation is observed in cerebral regions outside the visual area (and in more anterior slices as well). This argues against stimulation-induced motional artifacts. The lack of obvious motion of this type ("startle" response) was confirmed by direct observation during the stimulation of anesthetized mice outside the magnet. Probable motion artifacts—not correlated with the stimulation—were sometimes observed in images. Since these (not shown) appeared as positive enhancements rather bilaterally located near the inferior edge of the brain and along the edges of the two large cavities, we suspect that they represent ear twitches.

DISCUSSION

We can observe strong fMRI responses to photic stimulation, occurring in the occipital region of the brain of an anesthetized mouse. In other reports (4, 7), we have shown that this is possible in a time window between deep anesthesia and early arousal, during which the magnitudes of the responses grow exponentially (doubling time, ≈35 min) as time passes after a bolus pentobarbital administration.

Besides the temporal correlation with the stimulus, there are two other features suggesting that the positive fMRI changes we observe do in fact correspond to responses of the murine visual system. The first is that positive changes of the magnitudes seen in Figs. 3 and 4 are quite to be expected at the very high field strength of our experiment. Turner, *et al.* (1) report an increase of 6% at 1.5 T and 20% at 4.0 T for visual stimulation studies of the same (unanesthetized) human volunteer that kept the protocol as unchanged as possible. The different TE values employed (1) were used to calculate (14) the $\Delta R_2^* [(T_2^*)^{-1}_{\text{during response}} - (T_2^*)^{-1}_{\text{before or after response}}]$ values at 1.5 T and 4.0 T. The ratio $(\Delta R_2^*)_{4.0}/(\Delta R_2^*)_{1.5}$ was found to be 5 ± 1 (1), yielding an exponent of 1.6 for the $\mathbf{B}_0$-dependence (1). With this, the 6% change at 1.5 T (1) combines with the TE value of 11 ms that we employ to predict a 39% increase at 9.4 T. The average value of the six positive maxima in Fig. 3 is 40%. That we sometimes observe significantly larger changes (Fig. 3*a*) could simply be due to partial volume effects. Our ROI volumes are less than one-tenth of those of the lower-field experiments (1). The cutoff values (±7%) for the difference images in Fig. 4 are larger than the maximum changes observed in low-field studies. Because they are based on the baseline image pixel with maximum intensity, the percentage scales in Fig. 4 are more conservative than those of Fig. 3, which are based on the mean ROI pixel intensity of the average baseline image. (Recall that Figs. 3a and 4 are different presentations of the same data.) The second feature is the location of the positive changes. Electrophysiological studies have detected a region of cells that responds to binocular input, located in the center of the visual cortex in the left hemisphere, ≈1 mm from the midline (figure 2 of ref. 13). Because of the position and thickness of our fMRI slices (Fig. 1), it is not possible to further localize the positive changes we see (Fig. 4) to either the occipital surface of the left hemisphere of the cerebrum, or to some slightly deeper cortical layer in a somewhat more anterior position.

Almost all of the now many fMRI studies reported in the literature have been conducted on awake human subjects. With visual stimuli (reviewed in ref. 2), as with others, the fMRI responses are found to be *sustained* for the length of the stimulation and had been uniformly reported to be *positive* (ignoring occasional weak negative "undershoots" at the ends of some responses). Our results differ in each of these aspects. We consider them separately.

Differential Response. An aspect of our results unique for fMRI is that we see responses only when the light stimulus is

turned on or off, or when its intensity is changed (Figs. 2–4). However, firing rate increases of exactly the on and off nature have been observed in microelectrode recordings from individual area 17 neurons of the urethane-anesthetized mouse (figure 2 of ref. 15). These were induced by a stationary flashing stimulus subtending ≈10° of the receptive field (15). We estimate the size of our stimulus to be very similar (except that we surely also have significant reflected light from the glass support walls). The microelectrode responses fade with a characteristic time of ≈0.5 s (15), and this explains why we almost always see only one activated fMRI (acquisition time, 0.9 s) after each stimulus change (Figs. 2 and 3). Thus, we are directly detecting operations of the "M" ("luminance", or "broad-band") pathway (16) of the murine visual system. The other major channel of the vertebrate comprises the two "P" ("color-opponent") streams (17), which manifest a sustained response to the stimulus (18). The M channel provides excitatory signals for both increments and decrements in illumination. It is initiated with ON, OFF, and/or ON/OFF bipolar cells in the retinal ganglia of the vertebrate (16, 19). At least in the primate, the M pathway remains segregated in the geniculostriate system (18) before connecting to the primary visual cortex; but there, and after leaving the striate cortex, the separation is apparently not as distinct as once thought (20).

The brain actually responds to *perceived* intensity, or luminance; one of two primary sensory cues (17). The M pathway has also been studied with visual evoked potential responses in anesthetized cats (21). Though the overall pattern used to stimulate the cats remained isoluminant, the contrast—a measure of the difference of luminance values within a grating pattern—was varied (21). The response amplitude was approximately proportional to the logarithm of the absolute value of the contrast change in the stimulus. Our fMRI results also seem to reflect an absolute temporal (mathematical) differentiation of the intensity (I) of the light incident on the eye—i.e., they appear proportional to $|\partial I/\partial t|$ (Fig. 3). Spekreijse and coworkers (22) refer to the "differentiating network. . . .after rectification." Such a pathway quite likely employs some form of "adapted" membrane channel (23).

Individual cells in the M pathway show the prototypical ON/OFF responses (15). When one is studying signals that integrate the actions of many neurons, however, the P channel, usually operating contemporaneously with the M stream, causes an observed response that persists for the duration of the stimulus (18). This is the nature of the result that has been observed in every visual stimulation fMRI study of awake humans (cited in ref. 2) of which we are aware. Only one of the durations (2 s; ref. 24) was as short as our shortest (≈3.6 s), but the longest are greater than our longest (≈18 s). Essentially all studies have used a "flickering" light source with a flashing frequency of 6–8 Hz. The period of this oscillation (7^{-1} = 0.143 s, here; see top of Fig. 2) is much shorter than the typical image acquisition time (0.9 s, here); one would not be able to observe the physiological effects that occur with this frequency, if any (21). In many cases, the stimulus also "flickers" in the spatial sense (the "flickering checkerboard" sources). In these situations, the retinal image is spatially dynamic and so the M channel is being continually excited, and thus has the same sustained response as the P stream. However, our stimulus flickers only in the temporal sense. In some of the human activation studies, the stimulation seems somewhat similar to ours in this regard (although it is often not clear whether there is more than one "point"), and yet sustained responses are observed.

Why do we directly detect the M stream in our experiments? At least three hypotheses occur to us.

(*i*) A P channel is not excited. Perhaps our isochromatic stimulus does not excite a P channel. However, even when an awake subject is very still and nonblinking, uncontrolled eye movements cause the retinal image to be spatially dynamic even when the stimulus is not (21). Thus, a continually excited M channel yields a response that appears like that of a P channel. In the anesthetized cat visual evoked potential studies, the animals were also pharmaceutically paralyzed in order to suppress eye movements (21). Although pentobarbital is not thought of as a paralytic agent, it is quite possible that it does act as such at the high doses required for rodent studies. The dose used here is more than an order of magnitude greater than the human clinical dose (2–4 mg/kg; ref. 25). In examinations outside the NMR magnet, there were certainly no eye movements evident in the heavily anesthetized mouse. Studies of visual perception by the awake but paralyzed human have been made (26).

(*ii*) A P channel is not responsive. Perhaps the M pathway recovers from the effects of the anesthetic before a P channel does, which may not occur before the mouse exhibits significant motion. An intriguing locus for such a differential anesthesia effect could be the lateral geniculate nucleus of the thalamus, "the gateway to the cortex" (27). This is much closer to the brainstem, and the two pathways are certainly still separate in this brain structure. The M channel employs the two magnocellular layers while the P stream employs the four parvocellular layers (hence their names) of lateral geniculate nucleus neurons. Since different kinds of nerve cells are involved, it is not unreasonable to postulate that an anesthetic agent molecule could act differently on them (28). The lateral geniculate nucleus has been suggested as the possible site of suppression of the M pathway during saccadic eye movements (29). It is interesting that such suppression was historically characterized as a kind of "anesthesia" (30).

(*iii*) A P channel is not important. Perhaps the mice do not have a significant P pathway. After all, they are nocturnal animals for whom color-sensitivity and high spatial resolution are not so important. Such animals "have mainly receptors for dim light (rods)" (31). Indeed, Mangini and Pearlman (15) found that half of the area 17 neurons they studied with microelectrodes in the anesthetized mouse exhibited responses such as we see in Fig. 2; they refer to these as having nonoriented retinal receptive fields. It may be possible to test aspects of these hypotheses. With larger animals, one can administer a drug that selectively affects ON bipolar cells (16). One can also employ isoluminant or isochromatic stimuli that evoke the P or M pathways, respectively (29).

Negative fMRI Changes. Recently, Menon, *et al.* (2) have reported high-field (4 T) studies of visual stimulation in awake humans in which some pixels exhibit a very small negative fMRI change during the first 2–3 s of the response. This is followed by a switch to a larger positive change for the duration of the 10-s stimulation and for a few seconds thereafter. After the present paper was submitted, four abstracts have appeared that report sustained negative fMRI changes in some brain regions for cognitive/motor (32) and mental imagery (33) protocols with awake human subjects, and for visual stimulations of anesthetized monkeys (34) and awake humans (35).

The manifestation of the BOLD (blood oxygenation level dependent), or Ogawa, mechanism as a positive enhancement in fMRI has generally been interpreted as a reflection of *hyper*oxygenation of the blood in the ROI vasculature (14, 36). Thus, a negative change would naturally be considered to be a sign of *hypo*oxygenation.††

From the principles underlying the BOLD mechanism (36), we can make the following generalizations for the signal from water

††Strictly speaking, the use of the term *oxygenation* in this context is not appropriate. It connotes the *fraction* of blood hemoglobin iron that is oxygenated (1 minus the fraction that is deoxygenated). However, the quantity that is the main determinant of the bulk magnetic susceptibility of the blood is the actual *concentration* of deoxyhemoglobin-iron, [deoxyhemoglobin-iron$_{blood}$]. The concentration of oxyhemoglobin-iron makes almost no contribution (figure 15 of ref. 36).

spins around a blood vessel with a given orientation in $\mathbf{B}_0$. The most likely sources of a *positive* BOLD effect are an increase in blood oxygenation with a fixed vessel radius and/or a decrease in vessel radius with a fixed level of oxygenation, whereas for a *negative* BOLD effect, a decrease in blood oxygenation with a fixed vessel radius and/or an increase in vessel radius with a fixed level of oxygenation. However, it seems unlikely that capillary radii change during activation, if ever (37). Thus, in active (and inactive) capillary beds, changes in BOLD effects probably do reflect changes in blood oxygenation level (actually, the [deoxyhemoglobin-iron$_{blood}$] value). Arterioles, however (and probably also venules), can transiently change size during activation (38). The magnitude of an fMRI response based on a BOLD effect, moreover, also depends on the orientation of the vessel in $\mathbf{B}_0$ and the proximity of other vessels (36). Of course, any practical MRI ROI contains a large ensemble of vessels with distributions of sizes and orientations in $\mathbf{B}_0$ (36).

The average [deoxyhemoglobin-iron$_{blood}$] value in a capillary will decrease if any increase in aerobic glycolysis in the neurons surrounding it is more than compensated by an increase in the linear flow of blood through it. This would cause a positive BOLD effect—an increase in image intensity. This might happen in a capillary bed supplying the activated nerve cells but it could also happen (to an even greater extent) in capillary beds serving neurons enjoying no increase in activity but supplied by the same arterial system as the first capillary bed (39). This is possible because blood flow appears to be regulated by dilation at the arteriole (and probably venule) level (37). The hyperoxygenation of capillary beds by an increase in flow without a corresponding increase in neuronal activity is probably mimicked in experiments involving controlled periods of hypercapnia. These have been clearly shown to cause an increase in blood flow (37) on the one hand, and to give rise to a positive BOLD effect in fMRIs (40) on the other hand.

The average [deoxyhemoglobin-iron$_{blood}$] value in a capillary will increase if an increase in aerobic glycolysis in the neurons surrounding it is not compensated by an increase in the linear flow of blood through it. Since the BOLD mechanism is sensitive only to the concentration of the paramagnetic product of aerobic glycolysis, this would cause a negative BOLD effect; a decrease in image intensity. Because such a phenomenon would be expected to happen only in the capillary beds actually serving the neurons with increased activity, it would likely arise from a small region of tissue. Its measurement might be rendered difficult by partial volume effects, or impossible by larger positive BOLD effects from more extensive nearby regions in the same voxel. Our nominal voxel size ($\approx$220 nl) is only one-fifth of that ($\approx$1 μl) in even the highest resolution fMRI studies carried out on humans at 4 T (41), which is, in turn, an order of magnitude smaller than usual. This may help us to observe the negative fMRI changes that we do see.

The exact substrate of the negative fMRI changes observed (Fig. 4) is not known. Certainly, the superior sagittal sinus passes through the slice in this region. However, its tangent is fairly parallel to $\mathbf{B}_0$ at this point. A cylinder perfectly parallel to $\mathbf{B}_0$ gives absolutely no BOLD effect (36). Also, the conventional wisdom in the fMRI community is that a large draining vein gives rise to a positive BOLD effect. It is intriguing to note that the murine pineal gland is located in the region exhibiting the negative fMRI change (see the midsagittal view in Fig. 1).

We acknowledge Profs. Clifford Patlak, James Dilger, Joseph Fenstermacher, Neal Cohen, and Larry Abel, and Drs. Daniel Weinberger, Joseph Frascella, Joanna Fowler, Stephen Dewey, Alfred Wolf, Jing-Huei Lee, and Lawrence Latour for helpful discussions, as well as Prof. Philip Johnson for the optical fiber, and Dr. Mitchell Albert for help with initial mouse experiments. We thank the National Institutes of Health (Grant GM 32125 to C.S.S.) and the Laboratory Directed Research and Development Program of Brookhaven National Laboratory (grant to J.S.F. and C.S.S.) for support of these studies. Part of this work was carried out at Brookhaven National Laboratory under Contract DE-AC02-76CH00016 with the U.S. Department of Energy and supported by its Office of Health and Environmental Research.

1. Turner, R., Jezzard, P., Wen, H., Kwong, K. K., Le Bihan, D., Zeffiro, T. & Balaban, R. S. (1993) *Magn. Reson. Med.* **29,** 277–279.
2. Menon, R. S., Ogawa, S., Hu, X., Strupp, J. P., Andersen, P. & Ugurbil, K. (1995) *Magn. Reson. Med.* **33,** 453–459.
3. Hetherington, H. P., Luney, D. J. E., Vaughan, J. T., Pan, J. W., Ponder, S. L., Tschendel, O., Tweig, D. B. & Pohost, G. M. (1995) *Magn. Reson. Med.* **33,** 427–431.
4. Palyka, I., Huang, W., Eisenstein, E. M., Volkow, N. D. & Springer, C. S. (1996) *Hum. Brain Mapping* **4,** in press (abstr.).
5. Huang, W., Albert, M. S., Volkow, N. D. & Springer, C. S. (1993) *Proc. Soc. Magn. Reson. Med.* **12,** 1378 (abstr.).
6. Huang, W., Volkow, N. D., Eisenstein, E. M. & Springer, C. S. (1994) *Proc. Soc. Magn. Reson.* **2,** 689 (abstr.).
7. Huang, W., Palyka, I., Eisenstein, E. M., Volkow, N. D. & Springer, C. S. (1995) *Proc. Soc. Magn. Reson.* **3,** 783 (abstr.).
8. Palyka, I., Huang, W., Eisenstein, E. M., Volkow, N. D. & Springer, C. S. (1996) *Proc. Int. Soc. Magn. Reson. Med.* **4,** 1856 (abstr.).
9. Sidman, R. L., Angevine, J. B. & Pierce, E. T. (1971) *Atlas of the Mouse Brain and Spinal Cord* (Harvard Univ. Press, Cambridge, MA).
10. Gyngell, M. L. (1988) *Magn. Reson. Imaging* **6,** 415–419.
11. Frahm, J., Merboldt, K.-D., Haenicke, W., Kleinschmidt, A. & Boecker, H. (1994) *NMR Biomed.* **7,** 45–53.
12. Labadie, C., Lee, J.-H., Vetek, G. & Springer, C. S. (1994) *J. Magn. Reson. B* **105,** 99–112.
13. Pearlman, A. L. (1985) in *Cerebral Cortex*, eds. Peters, A. & Jones, E. G. (Plenum, New York), Vol. 3, pp. 1–18.
14. Albert, M. S., Huang, W., Lee, J.-H., Patlak, C. S. & Springer, C. S. (1993) *Magn. Reson. Med.* **29,** 700–708.
15. Mangini, N. J. & Pearlman, A. L. (1980) *J. Comp. Neurol.* **193,** 203–222.
16. Schiller, P. H. (1992) *Trends Neurosci.* **15,** 86–92.
17. DeYoe, E. A. & Van Essen, D. C. (1988) *Trends Neurosci.* **11,** 219–226.
18. Schiller, P. H. & Logothetis, N. K. (1990) *Trends Neurosci.* **13,** 392–398.
19. Lettvin, J. Y., Maturana, H. R., McCulloch, W. S. & Pitts, W. H. (1959) *Proc. Inst. Radio Eng.* **47,** 1940–1951.
20. Goodale, M. A. & Milner, A. D. (1992) *Trends Neurosci.* **15,** 20–25.
21. Pang, X. D. & Bonds, A. B. (1991) *Vision Res.* **31,** 1509–1516.
22. Padmos, P., Haaijman, J. J. & Spekreijse, H. (1973) *Electroencephalogr. Clin. Neurophysiol.* **35,** 153–163.
23. Hamill, O. P. & McBride, D. W. (1995) *Am. Sci.* **83,** 30–37.
24. Blamire, A. M., Ogawa, S., Ugurbil, K., Rothman, D., McCarthy, G., Ellerman, J. M., Hyder, F., Rattner, Z. & Shulman, R. G. (1992) *Proc. Natl. Acad. Sci. USA* **89,** 11069–11073.
25. Morgan, G. E. & Mikhail, M. S. (1992) *Clinical Anesthesiology* (Appleton & Lange, Norwalk, CT), 1st Ed., p. 122.
26. Matin, L., Picoult, E., Stevens, J. K., Edwards, McI. W., Young, D. & MacArthur, R. (1982) *Science* **216,** 198–201.
27. Crick, F. (1984) *Proc. Natl. Acad. Sci. USA* **81,** 4586–4590.
28. Franks, N. P. & Lieb, W. R. (1994) *Nature (London)* **367,** 607–614.
29. Burr, D. C., Morrone, M. C. & Ross, J. (1994) *Nature (London)* **371,** 511–513.
30. Morgan, M. J. (1994) *Nature (London)* **371,** 473.
31. Sterling, R. (1990) in *The Synaptic Organization of the Brain*, ed. Shepherd, G. M. (Oxford Univ. Press, New York), p. 172.
32. Scarth, G., McIntyre, M., Wowk, B. & Somorjai, R. (1995) *Proc. Soc. Magn. Reson* **3,** 238 (abstr.).
33. Le Bihan, D. & Dohi, M. (1995) *Proc. Soc. Magn. Reson.* **3,** 452 (abstr.).
34. Quast, M. J., Klinke, S. S., Deyo, D. & Wei, J. (1995) *Proc. Soc. Magn. Reson.* **3,** 60 (abstr.).
35. Mitra, P. P., Thompson, D. J., Ogawa, S., Hu, X. & Ugurbil, K. (1995) *Proc. Soc. Magn. Reson.* **3,** 817 (abstr.).
36. Springer, C. S. (1994) in *NMR in Physiology and Biomedicine*, ed. Gillies, R. J. (Academic, New York), pp. 75–99.
37. Chen, J.-L., Wei, L., Acuff, V., Bereczki, D., Hans, F.-J., Otsuka, T., Finnegan W., Patlak, C. & Fenstermacher, J. (1994) *Microvas. Res.* **48,** 190–211.
38. Ngai, A. C., Ro, K. R., Morii, S. & Winn, H. R. (1988) *Am. J. Physiol.* **254,** H133–H139.
39. Palyka, I., Huang, W. & Springer, C. S. (1995) *Bull. Magn. Reson.* **17,** 46–53.
40. Jezzard, P., Heineman, F., Taylor, J., DesPres, D., Wen, H., Balaban, R. S. & Turner, R. (1994) *NMR Biomed.* **7,** 35–44.
41. Ugurbil, K., Garwood, M., Ellerman, J., Hendrich, K., Hinke, R., Hu, X., Kim, S.-G., Menon, R., Merkle, H., Ogawa, S. & Salmi, R. (1993) *Magn. Reson. Q.* **9,** 259–277.